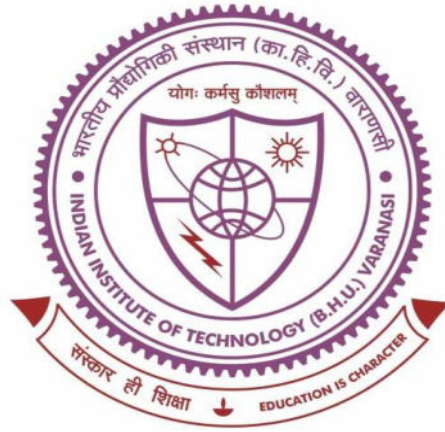


**STATIC AND SEISMIC STABILITY ANALYSIS OF
VARIOUS SLOPES AND RETAINED BACKFILLS BY
CONSIDERING CONSTANT/VARIABLE SATURATION
STATE**



A Thesis

Submitted for the Degree of
Doctor of Philosophy
In the Faculty of Engineering
By
Sourav Sarkar

Under the supervision of
Dr. Manash Chakraborty

**DEPARTMENT OF CIVIL ENGINEERING
INDIAN INSTITUTE OF TECHNOLOGY
BANARAS HINDU UNIVERSITY
VARANASI-221005
INDIA**

17061008

2023

CERTIFICATE

It is certified that the work contained in the thesis titled **“STATIC AND SEISMIC STABILITY ANALYSIS OF VARIOUS SLOPES AND RETAINED BACKFILLS BY CONSIDERING CONSTANT/VARIABLE SATURATION STATE.”** has been carried out under my supervision and this work has not been submitted elsewhere for a degree.

It is further certified that the student has been fulfilled all the requirements of Comprehensive Examination, Candidacy, and State of the Art (SOTA) for the award of Ph.D degree.

Dr. Manash Chakraborty

Supervisor

Asst. Professor

Dept. of Civil engineering

IIT(BHU)

Varanasi, U.P, India-221005

COPYRIGHT TRANSFER CERTIFICATE

Title of the Thesis: **STATIC AND SEISMIC STABILITY ANALYSIS OF VARIOUS SLOPES AND RETAINED BACKFILLS BY CONSIDERING CONSTANT/VARIABLE SATURATION STATE.**

Name of the Student: **Mr. Sourav sarkar**

Copyright Transfer

The undersigned hereby assigns to the Indian Institute of Technology, (BHU), Varanasi, all rights under copyright that may exist in and for the above thesis for the award of the Doctor of Philosophy.

Date:

Place: Varanasi

(Sourav sarkar)

Note: However, the author may reproduce or authorize others to reproduce material extracted verbatim from the thesis or derivative of the thesis for the author's personal use provided that the source and the Institute's copyright notice are indicated.

DECLARATIONS BY THE CANDIDATE

I, **SOURAV SARKAR**, certify that the work embodied in this thesis is my own bonafide work and carried out by me under the supervision of **Dr. Manash Chakraborty** from **July 2017 to July 2023** at the **Department of Civil Engineering, IIT(BHU), Varanasi**. The matter embodied in this has not been submitted for the award of any other degree/diploma. I declared that I have faithfully acknowledged and given credits to the research workers wherever their works have been cited in my work in this thesis. I further declare that I have not willfully copied any other's work, paragraphs, text, data, results, etc, reported in journals, book, magazines, reports dissertations, thesis, etc., or available at websites and included them in this thesis and cited as my own work.

Date:

Place: Varanasi

(Sourav sarkar)

CERTIFICATE BY THE SUPERVISOR

It is certified that the above statement made by the student is correct to the best of our knowledge.

Dr. Manash Chakraborty
Supervisor
Asst. Professor
Dept. of Civil Engineering
IIT(BHU)
Varanasi, U.P, India-221005

Dedicated to my
Friends & Family

ACKNOWLEDGMENT

First and foremost, I would like to express my deepest gratitude to Lord Shiva for blessing me with countless opportunities, knowledge, and unwavering support, enabling me to complete this thesis successfully. Though my name appears on the cover, the accomplishment of this dissertation would not have been possible without the assistance and guidance of numerous individuals, to whom I owe my heartfelt appreciation.

I am immensely grateful to my supervisor, **Dr. Manash Chakraborty**, from the Civil Engineering Department at IIT (BHU), Varanasi, for his exceptional guidance, continuous monitoring, and unwavering encouragement throughout the entire duration of this research work. I am indebted to Dr. Manash Chakraborty for his invaluable inspiration and helpful recommendations, which significantly contributed to the completion of my research.

I extend my sincere appreciation to the members of my RPEC, Dr. Bala Ramudu Paramkusam as the internal expert and Dr. Prateek Chattopadhyay as the external expert, for their valuable assistance, insightful suggestions, and constant encouragement during the entirety of my research work.

Furthermore, I would like to express my gratitude to Prof. Sasankasekhar Mandal, Head of the Department of Civil Engineering, Indian Institute of Technology (BHU), Varanasi, for providing the necessary facilities for my research. My heartfelt regards go to Prof. Arun Prasad, Dr. Bala Ramudu Paramkusam, Dr. Suresh Kumar, Dr. Supriya Mohanty, and all the faculty members of the Civil Engineering Department for their unconditional support throughout my academic journey.

Special gratitude is extended to Dr. Dharendra Pal of Precision Instruments for his innovative ideas and continuous guidance throughout the course of my work. I am also thankful to my friends and colleague, Dr. Nitesh Bonal, Mrs. Shivani Dhiriyan, Dr. Parul Rawat, Dr. Amit Kumar Ram, Mr. Surya Dev Prasad, Mr. Abhay Kumar, Mr. Amit Singh, Mr. Ankit Tiwari, Dr. Ajay Shankar Bangwal, Dr. Mohit Chaudhary for their thought-provoking discussions, unwavering support, cooperation, and assistance in various ways.

In particular, I would like to express my heartfelt appreciation to some senior Dr. Manish Kumar Mandal, Dr. Bables Kumar Jha, Dr. Rahul Singh, Dr. Sujeet Kumar, Dr. Abhishek Kumar, Dr. Satyajeet Mondal, Dr. Nitesh Gupta for their constant encouragement, love, and moral support. I take immense pleasure in sharing the credit for my research work with all my teachers who have played a significant role at different stages of my academic career.

Lastly, I am eternally grateful to my entire family for their unwavering faith, patience, encouragement, blessings, and unconditional love. My deepest appreciation goes to my father and my mother for their unwavering motivation, belief in me, and continuous support. A special thanks to my special family for always holding my hand through the ups and downs, providing unwavering support and love.

I am sincerely grateful to each and every individual mentioned above, as well as those who have supported me in various ways, for their invaluable contributions to the completion of this thesis.

Sourav Sarkar

CONTENTS

ACKNOWLEDGMENT	iii
ABSTRACT	v
CONTENTS	xi
LIST OF FIGURES	xix
LIST OF TABLES	xxvii
LIST OF NOTATIONS	xxxi
Chapter 1 INTRODUCTION	1
1.1 GENERAL	1
1.2 MOTIVATION FOR THE PRESENT RESEARCH	3
1.3 ORGANIZATION OF THE THESIS	6
Chapter 2 LITERATURE REVIEW	9
2.1 INTRODUCTION	9
2.2 LITERATURE REVIEW: VARIATIONAL METHOD AND UPPER BOUND RIGID BLOCK METHOD	9
2.2.1 Variational Method	9
2.2.1.1 Goldshtein et al. (1969)	10
2.2.1.2 Kogan and Lupashko (1970)	10
2.2.1.3 Narayan (1975)	10
2.2.1.4 Revilla and Castillo (1977)	11
2.2.1.5 Baker and Garber (1978)	11
2.2.1.6 Castillo and Luceno (1982)	11
2.2.1.7 Leshchinsky and Reinschmidt (1985)	11
2.2.1.8 Dixit and Mandal (1992)	12
2.2.1.9 Leshchinsky and San (1994)	12
2.2.1.10 Ling et al. (1997)	12
2.2.1.11 Baker (2003)	12
2.2.1.12 Baker et al. (2006)	13
2.2.1.13 Chen et al. (2016)	13
2.2.1.14 Onyelowe KC (2017)	14
2.2.1.15 Li et al. (2018)	14
2.2.1.16 Hua et al. (2022)	15
2.2.1.17 Fengxi et al. (2023)	15

2.2.2 Upper bound rigid block method	16
2.2.2.1 Chen et al. (1969)	16
2.2.2.2 Chen and Giger (1971)	16
2.2.2.3 Chen (1975)	16
2.2.2.4 Michalowski (1989)	16
2.2.2.5 Michalowski (1995)	17
2.2.2.6 Donald and Chen (1997)	17
2.2.2.7 Farzaneh and Askari (2003)	17
2.2.2.8 Kumar and Samui (2006)	18
2.2.2.9 Farzaneh et al. (2008)	18
2.2.2.10 Michalowski and Nadukuru (2013)	18
2.2.2.11 Gao et al. (2014)	18
2.2.2.12 Zhao et al. (2016)	19
2.2.2.13 Li and Yang (2019)	19
2.2.2.14 Li et al. (2021)	19
2.2.2.15 Zuo et al. (2022)	20
2.3 LITERATURE REVIEW ON UNSATURATED MECHANICS AND APPLICATIONS	20
2.3.1 Hilf (1956)	21
2.3.2 Jennings and Burland (1962)	21
2.3.3 Fredland et al. (1978)	22
2.3.4 van Genuchten (1980)	22
2.3.5 Fredlund and Xing (1994)	22
2.3.6 Vanapalli and Fredlund (1996)	23
2.3.7 Tekinsoy et al. (2004)	23
2.3.8 Sheng et al. (2009)	24
2.3.9 Kim and Borden (2011)	24
2.3.10 Fredlund (2018)	25
2.3.11 Vahedifard et al. (2016)	25
2.3.12 Sun et al. (2019)	26
2.4 SUMMARY	26
Chapter 3 VARIATIONAL METHOD FOR ANALYZING SEISMIC STABILITY OF VARIAOUS SOIL SLOPES	29
3.1 INTRODUCTION AND REVIEW OF EXISTING STUDIES	29
3.2 PROBLEM STATEMENT	32

3.3	ANALYSIS PROCEDURE	33
3.3.1	Step 1: Obtaining the discrete formulation of F	34
3.3.2	Step 2: Transforming the discrete formulations into integral form	36
3.3.3	Step 3: Identifying the functional forms	39
3.3.4	Step 4: Employing the Euler-Lagrangian equation to obtain the expression of F_s	40
3.3.5	Step 5: Integrating (twice) the expression of F_s to obtain the form of slip surfaces	41
3.3.6	Step 6: Evaluating the unknown parameters of Step 5	42
3.3.6.1	Determining the integration constants and the stability number	43
3.3.6.2	Determining the intersection points	43
3.4	RESULTS AND DISCUSSIONS	47
3.4.1	Case 1: Homogeneous c - ϕ soil	48
3.4.2	Case 2: Non-homogeneous undrained cohesive soil ($\phi_u=0^\circ$)	49
3.4.3	Case 3: Two layered cohesive-frictional soil	54
3.4.4	Case 4: Homogeneous c - ϕ soil underlain by non-homogeneous Clays	59
3.5	VERIFICATIONS WITH EXISTING LITERATURES	67
3.5.1	Case 1: Homogeneous c - ϕ soil	67
3.5.2	Case 2: Non-homogeneous undrained cohesive soil ($\phi_u=0^\circ$)	69
3.5.3	Case 3: Two layered cohesive-frictional soil	71
3.5.4	Case 4: Homogeneous c - ϕ soil underlain by non-homogeneous clays	72
3.6	SUMMARY	74
3.7	LIMITATIONS	75

Chapter 4 VARIATIONAL METHOD FOR ANALYZING SEISMIC STABILITY

OF ROCK SLOPES	77
4.1 INTRODUCTION AND REVIEW OF EXISTING STUDIES	77
4.2 PROBLEM STATEMENT FOR ROCK SLOPE	78
4.3 HOEK-BROWN FAILURE CRITERION	79
4.4 ANALYSIS	82
4.5 RESULTS AND DISCUSSIONS	87

4.5.1 Influence of slope geometry (β and h)	88
4.5.2 Influence of rock properties (m_i , GSI , and σ_{ci})	89
4.5.3 Influence of horizontal seismic forces (k_h)	96
4.6 COMPARISON OF RESULTS	98
4.6.1 Comparison of the present solutions obtained by Hoek et al. (2000) and li et al. (2008)'s proposition regarding σ'_{3max}	99
4.6.2 Comparison of the present solutions with the solutions available in the literature	100
4.7 SUMMARY	109
4.8 LIMITATIONS	109
Chapter 5 STRENGTH REDUCTION METHOD FOR ANALYZING STABILITY OF TWO-LAYERED SOIL SLOPES	111
5.1 INTRODUCTION AND REVIEW OF EXISTING STUDIES	111
5.2 STRENGTH REDUCTION METHOD (SRM)	112
5.3 PROBLEM STATEMENT AND METHODOLOGY	114
5.4 RESULTS AND DISCUSSIONS	115
5.5 COMPARISON OF RESULTS	125
5.6 SUMMARY	131
5.7 LIMITATIONS	131
Chapter 6 VARIATIONAL METHOD FOR UNSATURATED SOIL SLOPES	133
6.1 INTRODUCTION AND REVIEW OF EXISTING STUDIES	133
6.2 PROBLEM STATEMENT AND CONSIDERED ASSUMPTIONS	134
6.2.1 Suction-stress, vG-SWCC, Gd-SWCC, Gd-HCF, and MMC	136
6.2.2 Steady-State Flow	141
6.2.3 Transient State Flow	144
6.3 FORMULATIONS	148
6.4 ANALYSIS TECHNIQUES	152
6.5 RESULTS AND DISCUSSIONS	157
6.5.1 Influence of slope geometry (β and h)	159
6.5.2 Influence of material parameters (ϕ , $1/\alpha$, n , and m)	161
6.5.3 Influence of flow conditions and water table position	166
6.5.4 Failure pattern	168
6.6 COMPARISONS OF RESULTS	172
6.7 SUMMARY	174

6.8	LIMITATIONS	175
Chapter 7 UPPER BOUND RIGID BLOCK METHOD FOR UNSATURATED SOIL SLOPES UNDER SEISMIC AND SURCHARGE LOADING CONDITIONS		
		177
7.1	INTRODUCTION AND REVIEW OF EXISTING STUDIES	177
7.2	PROBLEM STATEMENT AND MODEL FORMULATION	178
7.3	UPPER BOUND LIMIT ANALYSIS	179
7.3.1	Overview	179
7.3.2	Collapse mechanism and formulations	181
7.3.2.1	Rate of external work done (\dot{W})	182
7.3.2.1.1	Due to the gravitational forces (\dot{W}_{weight})	182
7.3.2.1.2	Due to the application of seismic forces ($\dot{W}_{earthquake}$)	183
7.3.2.1.3	Due to the application of surcharge pressure ($\dot{W}_{surcharge}$)	183
7.3.2.2	Rate of energy dissipation	184
7.3.2.2.1	Due to the internal cohesion ($\dot{D}_{cohesion}$)	184
7.3.2.2.2	Due to the suction ($\dot{D}_{suction}$)	185
7.3.2.3	Determining the stability number by equating $\dot{W} = \dot{D}$	186
7.3.2.3.1	For pseudo-static force	186
7.3.2.3.2	For surcharge loads (without pseudo-static forces)	187
7.3.3	Stability number and numerical tool	188
7.4	PARAMETRIC STUDY	189
7.4.1	Impact of β and ϕ' on S_n	189
7.4.2	Impact of λ on S_n	192
7.4.3	Impact of water table depth h_w on S_n	194
7.4.4	Combined impact of k_h and h_w on S_n	196
7.4.5	Impact of surcharge load (p_s) on S_n	196
7.5	FAILURE SURFACES	199
7.6	COMPARISON WITH LITERATURE	199

7.7	SUMMARY	204
7.8	LIMITATIONS	205
Chapter 8	STATIC AND SEISMIC LATERAL EARTH PRESSURES FOR RETAINING WALL BACKFILLED WITH UNSATURATED SOIL UNDER STEADY-STATE FLOW	207
8.1	INTRODUCTION AND REVIEW OF EXISTING STUDIES	207
8.2	MODIFICATION AND APPLICATION OF RANKINE'S METHOD FOR ADDRESSING VERTICAL RETAINING WALL SUPPORTING UNSATURATED BACKFILL WITH HORIZONTAL SURFACE	209
8.2.1	Construction of Rankine's based closed-form expression for unsaturated backfills	209
8.2.1.1	Computation of earth pressure (EP) coefficients	209
8.2.1.1.1	At Rest State	210
8.2.1.1.2	At Active State	210
8.2.1.1.3	At Passive State	211
8.2.1.2	Computation of tensile crack depth	213
8.2.2	Strategy of relaxing m -parameter and incorporating two-parameter HCF	214
8.2.3	Problem statement and involved assumptions	215
8.2.4	RESULTS AND DISCUSSIONS	216
8.2.4.1	Impact of m parameter	218
8.2.4.1.1	Variations of K_{0u} , K_{au} and K_{pu} for defined k_s	218
8.2.4.1.2	Variations of K_{0u} , K_{au} , and K_{pu} for specific Q	219
8.2.4.1.3	Crack Depth profiles versus α	224
8.2.4.1.4	Crack Depth profiles varying with Q	225
8.2.4.1.5	Total active earth pressure profiles - Active State	230
8.2.4.1.6	Component of Earth pressure Due to suction stress Passive state	231
8.2.4.2	Effect of Gardener's two parameter HCF model (1958)	235

8.3 MODIFICATION AND APPLICATION OF COULOMB'S METHOD FOR ADDRESSING INCLINED RETAINING WALL SUPPORTING UNSATURATED BACKFILL WITH INCLINED SURFACE	238
8.3.1 Problem statement	238
8.3.2 Formulations	238
8.3.2.1 Determination of seismic active earth pressure coefficient on unsaturated soil (K_{aue})	240
8.3.2.2 Deducing seismic active earth pressure distribution along depth ($p_{aue}(z)$) on unsaturated soil	241
8.3.3 Results and Discussions	242
8.3.3.1 Impact of backfill inclination (i) on critical Failure angle (ζ_{cr})	243
8.3.3.2 Impact of backfill inclination (i) on area of failure wedge (A_f)	243
8.3.3.3 Impact of backfill inclination and pseudo-static forces on K_{aue}	245
8.3.3.4 Impact of friction angle (ϕ') on K_{aue}	245
8.3.3.5 Impact of wall inclination angle (β) on K_{aue}	248
8.3.3.6 Impact of vG model parameters on K_{aue}	248
8.3.3.7 Impact of water table depth (h_w) on K_{aue}	252
8.3.3.8 Impact of δ on coefficient of K_{aue}	252
8.3.3.9 Failure surfaces	255
8.3.4 Verification	257
8.4 SUMMARY	258
8.5 LIMITATIONS	259
Chapter 9 SEISMIC LATERAL EARTH PRESSURES FOR RETAINING WALL BACKFILLED WITH UNSATURATED SOIL UNDER TRANSIENT FLOW	261
9.1 INTRODUCTION AND REVIEW OF EXISTING STUDIES	261
9.2 PROBLEM STATEMENT AND CONSIDERED ASSUMPTIONS	262
9.3 METHODOLOGY	264
9.3.1 Computation of lateral earth pressure	264
9.3.2.1 Step 1: Computation of suction stress	264

9.3.1.2 Step 2: Computation of earth pressure under Transient flow for seismic condition	266
9.3.2 Computation of tension crack depth	268
9.4 FAILURE CIRCLES AND ENVELOPES	270
9.5 PRESSURE PROFILES	270
9.5.1 Pore-water pressure and suction stress profiles	274
9.5.2 Earth pressure profiles for static conditions	276
9.5.3 Earth pressure profiles for seismic conditions	281
9.6 CRACK DEPTH VARIATION	282
9.7 SUMMARY	286
9.8 LIMITATIONS	286
Chapter 10 CONCLUSIONS AND FUTURE SCOPE	287
10.1 CONCLUSIONS	287
10.2 SCOPE FOR FUTURE WORK	292
REFERENCES	295
Appendix-A: DERIVATION OF MATRIC SUCTION FOR STEADY-STATE FLOW AND GOVERNING DIFFERENTIAL EQUATION FOR TRANSIENT	307
Appendix-B: DERIVATION OF MUALEM'S AND BURDINE'S HCF MODELS	313
Appendix-C: DERIVATION OF MATRIC SUCTION AND SUCTION STRESS BY USING TWO PARAMETER HCF MODEL	315
LIST OF PUBLICATIONS	317

LIST OF FIGURES

Fig. No.	Title	Page No.
Fig. 3.1	Schematic diagram of considered slopes for (a) Case 1, (b) Case 2, (c) Case 3, and (d) Case 4.	33
Fig. 3.2	(a) Arbitrary slip surface with n number of discretized segments, (b) force distribution in any arbitrary i^{th} slice.	35
Fig. 3.3	Form of the failure slip surface computed by variational method for (a) Case 1, 2 and (b) Case 3, 4.	37
Fig. 3.4	Algorithm flowchart for the Newton-Raphson method	47
Fig. 3.5	Variation of critical factor of safety with k_h for: (a) $\beta=25^\circ$; (b) $\beta=35^\circ$; (c) $\beta=55^\circ$; (d) $\beta=65^\circ$.	50
Fig. 3.6	Form of the critical slip surfaces for: (a) $\beta=60^\circ$, $k_h=k_v=0$; (b) $\beta=60^\circ$, $k_h=0.3, k_v=0$; (c) $\beta=60^\circ$, $k_h=k_v=0.3$; (d) $\beta=80^\circ$, $k_h=k_v=0$; (e) $\beta=80^\circ$, $k_h=0.3, k_v=0$; and (f) $\beta=80^\circ$, $k_h=k_v=0.3$.	51
Fig. 3.7	Variation of critical factor of safety (F_s) with k_h for: (a) $\beta=20^\circ$; (b) $\beta=30^\circ$; (c) $\beta=40^\circ$; (d) $\beta=50^\circ$.	53
Fig. 3.8	Form of the critical slip surfaces for: (a) $\beta=20^\circ$, $\lambda=3, k_v=0$; (b) $\beta=40^\circ$, $\lambda=3, k_v=0$; (c) $\beta=60^\circ$, $\lambda=3, k_v=0$; (d) $\beta=80^\circ$, $\lambda=3, k_v=0$.	55
Fig. 3.9	Variation of stability number with k_h for Case A soil with: (a) $\beta=45^\circ$; (b) $\beta=55^\circ$; (c) $\beta=65^\circ$; (d) $\beta=75^\circ$.	56
Fig. 3.10	Variation of stability number with k_h for Case B soil with: (a) $\beta=45^\circ$; (b) $\beta=55^\circ$; (c) $\beta=65^\circ$; (d) $\beta=75^\circ$.	57
Fig. 3.11	Form of the critical slip surfaces for: (a) $\beta=55^\circ$, $k_h=k_v=0$; (b) $\beta=55^\circ$, $k_h=0.3, k_v=0$; (c) $\beta=55^\circ$, $k_h=k_v=0.3$; (d) $\beta=75^\circ$, $k_h=k_v=0$; (e) $\beta=75^\circ$, $k_h=0.3, k_v=0$; and (f) $\beta=75^\circ$, $k_h=k_v=0.3$ subjected to $\phi_1=18^\circ$ and $\phi_2=30^\circ$.	58
Fig. 3.12	Variation of critical factor of safety (F_s) with k_h for: (a) $\beta=20^\circ$; (b) $\beta=30^\circ$; (c) $\beta=40^\circ$; (d) $\beta=50^\circ$ corresponding to $\alpha_1=0.2$.	66
Fig. 3.13	Variation of critical factor of safety (F_s) with k_h for: (a) $\beta=20^\circ$; (b) $\beta=30^\circ$; (c) $\beta=40^\circ$; (d) $\beta=50^\circ$ corresponding to $\alpha_1=0.6$.	67
Fig. 3.14	Form of the critical slip surfaces for: (a) $\beta=20^\circ$, $\lambda=3, \alpha_1=0.4, k_v=0$; (b) $\beta=40^\circ$, $\lambda=3, \alpha_1=0.4, k_v=0$; (c) $\beta=60^\circ$, $\lambda=3, \alpha_1=0.4, k_v=0$; (d) $\beta=80^\circ$, $\lambda=3, \alpha_1=0.4, k_v=0$.	68
Fig. 4.1	Schematic diagram of rectilinear rock slope.	79
Fig. 4.2	Graphical representation of GHB (Hoek et al. 2002) and EMC (Hoek et al. 2002; Li et al. 2008) for different GSI and m_i corresponding to (a) $\beta < 45^\circ$ and (b) $\beta \geq 45^\circ$.	84
Fig. 4.3	The variation of F_s with m_i for $h=20\text{m}$ with k_h equals to (a, d) 0.0; (b, e) 0.2 and (c, f) 0.4 correspond to two σ_{ci} , namely, 25 and 250 Mpa.	92

Fig. 4.4	Form of the critical slip surfaces for $h=20\text{m}$ with k_h equals to (a,d) 0.0; (b,e) 0.2; and (c,f) 0.4 and correspond to two β , namely, 55° and 75°	93
Fig. 4.5	Form of the critical slip surfaces for $h=100\text{m}$ with (a) $\beta=55^\circ$, $k_h=0$; (b) $\beta=55^\circ$, $k_h=0.4$; (c) $\beta=75^\circ$, $k_h=0$; and (d) $\beta=75^\circ$, $k_h=0.4$.	94
Fig. 4.6	The variation of c_{eq}/σ_{ci} with GSI and m_i for σ_{ci} equals to (a) 25 MPa and (b) 250 MPa.	95
Fig. 4.7	Form of the critical slip surfaces for $h=100\text{m}$ and $\beta=75^\circ$ with (a) $\sigma_{ci}=25\text{MPa}$, $k_h=0$; (b) $\sigma_{ci}=25\text{MPa}$, $k_h=0.4$; (c) $\sigma_{ci}=250\text{MPa}$, $k_h=0$; and (d) $\sigma_{ci}=250\text{MPa}$, $k_h=0.4$.	98
Fig. 4.8	The percentage difference of F_s by using formulation of Hoek et al. (2002) and Li et al. (2008) with β for different GSI corresponding to varying k_h with $\sigma_{ci}=250$ MPa.	100
Fig. 4.9	Comparison of the obtained critical slip surfaces with the prescribed slip surface provided by (a) Dong-ping et al. (2017) considering deep slip surface, (b) Dong-ping et al. (2017) considering shallow slip surface, and, (c) Li et al. (2008).	108
Fig. 5.1	Schematic diagram and the boundary conditions of a two-layered soil slope.	115
Fig. 5.2	The variation of F_s with t/D for a two-layered slope ($\beta=25^\circ$) corresponding to varying c_2 and (a) $c_1=0$ kPa, $\phi_1=40^\circ$, $\phi_2=25^\circ$, (b) $c_1=0$ kPa, $\phi_1=45^\circ$, $\phi_2=25^\circ$, (c) $c_1=8$ kPa, $\phi_1=40^\circ$, $\phi_2=25^\circ$ and (d) $c_1=8$ kPa, $\phi_1=45^\circ$, $\phi_2=25^\circ$.	121
Fig. 5.3	The variation of F_s with t/D for two different layered slopes ($\beta=25^\circ$ and 45°) corresponding to varying c_2 and (a) $c_1=8$ kPa, $\phi_1=35^\circ$, $\phi_2=20^\circ$ and (b) $c_1=8$ kPa, $\phi_1=35^\circ$, $\phi_2=30^\circ$.	122
Fig. 5.4	Adaptive mesh patterns at the collapse state for three different slopes: (a) $\beta=25^\circ$, (b) $\beta=35^\circ$ and (c) $\beta=45^\circ$.	123
Fig. 5.5	Adaptive mesh patterns at the collapse state by varying the top layer thickness: (a) $t=0.2D$, (b) $t=0.5D$ and (c) $t=0.8D$.	124
Fig. 5.6	Adaptive mesh patterns at the collapse state by varying the top layer frictional strength: (a) $\phi_1=35^\circ$, (b) $\phi_1=40^\circ$ and (c) $\phi_1=45^\circ$.	125
Fig. 6.1	Schematic representation of the chosen unsaturated soil slope of angle β along with the force distribution in two arbitrary slices.	135
Fig. 6.2	Impact of air entry value, saturation state, and the residual state on the (a) $\theta-\psi$, (b) $\Theta_n(\Theta_d)-\psi$, (c) $k-\psi$, and (d) $k_r-\psi$.	140
Fig. 6.3	Effect of suction stress on the structure of MC yield envelope and MC yield surface.	141
Fig. 6.4	The shear strength failure envelope in different (a) three-dimensional stress spaces, namely, $\tau-\psi-\sigma$ and $\tau-\sigma^s-\sigma$, and (b) two-dimensional stress planes, namely, $\tau-\psi$ and $\tau-\sigma^s$.	143

Fig. 6.5	The variation of σ^s with the distance above water table (z) corresponding to (a-d) steady state flow with different values of α :(a-b) $\alpha = 0.01 \text{ kPa}^{-1}$, (c) $\alpha = 0.1 \text{ kPa}^{-1}$, and (d) $\alpha = 0.3 \text{ kPa}^{-1}$.	145
Fig. 6.6	The σ^s profiles obtained from vG and Gardner's SWCC model corresponding to various infiltration rates.	146
Fig. 6.7	Limiting envelopes of m_1 , m_2 with respect to Δt for sand.	149
Fig. 6.8	The variation of σ^s with the distance above water table (z) corresponding to transient flow.	150
Fig. 6.9	Flowchart for the present iteration technique.	158
Fig. 6.10	The variation of N with slope angle, β , for three different slope height and subjected to (a-c) steady-infiltration and (d-f) steady-evaporation.	160
Fig. 6.11	The variation of N with frictional strength for two different R_M and three different steady-state flow, namely, (a, b) no flow ($q=0$); (c, d) infiltration ($q=-0.4k_s$); and (e, f) evaporation ($q=0.4k_s$).	162
Fig. 6.12	The variation of N with the inverse of α corresponding to three different slope height h , namely, 4m, 7m, and 10m and subjected to (a-c) no flow ($q = 0$) and (d-f) steady-state infiltration ($q = -3.14 \times 10^{-8} \text{ m/s}$).	163
Fig. 6.13	The variation of N with α^{-1} corresponding to two R_M 's and subjected to: (a, b) no flow condition ($q = 0$) (c, d) steady-infiltration ($q = -0.8k_s$) and (e, f) steady-evaporation ($q = 0.8k_s$).	165
Fig. 6.14	The variation of N , corresponds to steady-state and transient flow, with respect to the (a-b) soil friction angle, and (c-d) time.	168
Fig. 6.15	The variation of N with respect to the water-table position pertaining to three slopes ($\beta = 45^\circ, 60^\circ, 75^\circ$) and three steady-state flows ($q=0, -3.14 \times 10^{-8} \text{ m/s}, 1.15 \times 10^{-8} \text{ m/s}$).	169
Fig. 6.16	The evolution of critical failure surface through the numerical iteration corresponding to unsaturated soil slopes having (a) $\beta=35^\circ, \alpha=0.01 \text{ kPa}^{-1}, \phi=30^\circ$; (b) $\beta=75^\circ, \alpha=0.01 \text{ kPa}^{-1}, \phi=30^\circ$; (c) $\beta=35^\circ, \alpha=0.01 \text{ kPa}^{-1}, \phi=40^\circ$; (d) $\beta=35^\circ, \alpha=0.1 \text{ kPa}^{-1}, \phi=40^\circ$.	170
Fig. 6.17	The evolution of critical failure surface for two different m and n relationships (a, b, c) $R_M=0$ and (d, e, f) $R_M=2$ and subjected to three steady-state flows: (a,d) $q=0$, (b,e) $q=0.8k_s$, and (c,f) $q=-0.8k_s$.	171
Fig. 6.18	The evolution of critical failure surface for transient flow corresponding to t equals to: (a) 10 days, (b) 100 days, and (c) 400 days.	172

Fig. 7.1	Schematic representation of the chosen unsaturated soil slope of angle β subjected to: (a) seismic activity without surcharge, (b) surcharge load without any seismic forces.	180
Fig. 7.2	The variation of S_n with β and ϕ' corresponding to $k_h=0.1$ and λ equals to: (a,c,e) 0 and (b,d,f) 1, with three different α 's (kPa ⁻¹): (a,b) $\alpha=0.1$, (c,d) $\alpha=0.01$, and (e,f) $\alpha=0.001$.	190
Fig. 7.3	The form of $S_n(\beta)$ and $S_n(\phi')$ curves corresponding to $k_h=0.3$ and λ equals to: (a,c,e) 0 and (b,d,f) 1, with three different α 's (kPa ⁻¹): (a,b) $\alpha=0.1$, (c,d) $\alpha=0.01$, and (e,f) $\alpha=0.001$.	191
Fig. 7.4	The form of $S_n(\lambda)$ curves corresponding to various combinations of vG -model parameters: (a) $n=2.0$, $\alpha=0.1$ kPa ⁻¹ , (b) $n=7.0$, $\alpha=0.1$ kPa ⁻¹ , (c) $n=2.0$, $\alpha=0.01$ kPa ⁻¹ , (d) $n=7.0$, $\alpha=0.01$ kPa ⁻¹ , (e) $n=2.0$, $\alpha=0.001$ kPa ⁻¹ , and (f) $n=7.0$, $\alpha=0.001$ kPa ⁻¹ .	193
Fig. 7.5	The form of $S_n(h_w)$ curves corresponding to various combinations of vG n -parameter: (a, d, g) $n=2.0$, (b,e,h) $n=4.0$, (c,f,i) $n=7.0$ and vG α -parameter: (a,b,c) $\alpha=0.1$ kPa ⁻¹ , (d,e,f) $\alpha=0.01$ kPa ⁻¹ , and (g,h,i) $\alpha=0.001$ kPa ⁻¹ .	195
Fig. 7.6	The three-dimensional stability profiles in $S_n - k_h - h_w$ space for three different α 's: (a,b) $\alpha=0.1$ kPa ⁻¹ , (c,d) $\alpha=0.01$ kPa ⁻¹ , and (e,f) $\alpha=0.001$ kPa ⁻¹ and two λ 's (a,c,e) $\lambda=0$ and (b,d,f) $\lambda=1$.	197
Fig. 7.7	Variation of S_n with surcharge load p_s with respect to (a) and (b) vG parameter n ; (c) and (d) vG parameter α .	198
Fig. 7.8	Three dimensional representation of the variation of S_n with vG parameter α and p_s conforming to the parameters: $\phi'=25^\circ$, $Q=-0.4$, $\beta=45^\circ$ for (a) $h_w = 4.0$ m and (b) $h_w = 0$ m.	200
Fig. 7.9	The form of the developed failure surfaces corresponding to $\beta=45^\circ$, $\phi'=20^\circ$, $h_w=0$ m, $n=3.0$ and conforming to (a) $\alpha=0.1$ kPa ⁻¹ ; $\lambda=0$, (b) $\alpha=0.1$ kPa ⁻¹ ; $\lambda=1$, (c) $\alpha=0.01$ kPa ⁻¹ ; $\lambda=0$, (d) $\alpha=0.01$ kPa ⁻¹ ; $\lambda=1$, (e) $\alpha=0.001$ kPa ⁻¹ ; $\lambda=0$, (f) $\alpha=0.001$ kPa ⁻¹ ; $\lambda=1$.	201
Fig. 7.10	Log-spiral failure surfaces generated for two soil types, namely, an unsaturated soil ($\alpha=0.005$ kPa ⁻¹ , $n=2.0$) and a saturated soil (no suction) for the representative slope with geometric parameters: $\beta=70^\circ$, $\phi'=25^\circ$. The surfaces generated with the present analysis are compared with that of Vahedifard et al. (2016).	202
Fig. 7.11	A comparison of stability number obtained from present study with the solution of Sun et al. (2019) and Vahedifard et al. (2016) considering (a) $\alpha=0.005$ kPa ⁻¹ and (b) $\alpha=0.1$ kPa ⁻¹ .	203
Fig. 7.12	A comparison of stability number obtained from present study and the solution of Zhao et al. (2016) for different k_h .	204

- Fig. 8.1** (a) Schematic representation of unsaturated soil-backfill with matric suction variation (b) bounded surface in three-dimensional semi-logarithmic α - Q - z space demarcating the real and the complex zones (c) Mohr-Coulomb failure circles and corresponding failure envelopes along with the components of active and passive stress state distribution. 212
- Fig. 8.2** (a) The combined set of m and n parameters chosen in the analysis, (b) schematic representation of Gardner's one-parameter and two-parameter HCF models, and (c) variation of ξ for ensuring the similarity between OPM and TPM. 217
- Fig. 8.3** The variation of K_{ou} , K_{au} and K_{pu} in the vadose zone for (a, c, e) sands, and (b, d, f) clays. 220
- Fig. 8.4** The variation of K_{ou} above the water table for two α 's with various m 's and corresponding to (a) $n=2$, $Q=-0.4$; (b) $n=2$, $Q=0$; (c) $n=2$, $Q=0.4$; (d) $n=6$, $Q=-0.4$; (e) $n=6$, $Q=0$; (f) $n=6$, $Q=0.4$. 221
- Fig. 8.5** The variation of K_{au} above the water table for two α 's with various m 's and corresponding to (a) $n=2$, $Q=-0.4$; (b) $n=2$, $Q=0$; (c) $n=2$, $Q=0.4$; (d) $n=6$, $Q=-0.4$; (e) $n=6$, $Q=0$; (f) $n=6$, $Q=0.4$. 222
- Fig. 8.6** The variation of K_{pu} above the water table for two α 's with various m 's and corresponding to (a) $n=2$, $Q=-0.4$; (b) $n=2$, $Q=0$; (c) $n=2$, $Q=0.4$; (d) $n=6$, $Q=-0.4$; (e) $n=6$, $Q=0$; (f) $n=6$, $Q=0.4$. 223
- Fig. 8.7** The variation of crack depth with α for various m subjected to rest condition and corresponding to (a) $n=2.5$, $Q=0$; (b) $n=4.5$, $Q=0$; (c) $n=8.5$, $Q=0$; (d) $n=2.5$, $Q=-0.4$; (e) $n=4.5$, $Q=-0.4$; (f) $n=8.5$, $Q=-0.4$. 226
- Fig. 8.8** The variation of crack depth with α for various m subjected to active condition and corresponding to (a) $n=2.5$, $Q=0$; (b) $n=4.5$, $Q=0$; (c) $n=8.5$, $Q=0$; (d) $n=2.5$, $Q=-0.4$; (e) $n=4.5$, $Q=-0.4$; (f) $n=8.5$, $Q=-0.4$. 227
- Fig. 8.9** The variation of crack depth with α for different ϕ' and m subjected to active condition and corresponding to (a) $Q=0$; (b) $Q=-0.4$. 228
- Fig. 8.10** The variation of crack depth with Q for various m subjected to rest condition ((a) $n=1.1$, $\alpha=0.005$, (c) $n=1.1$, $\alpha=0.01$, (e) $n=6.5$, $\alpha=0.01$) and active condition ((b) $n=1.1$, $\alpha=0.005$, (d) $n=1.1$, $\alpha=0.01$, (f) $n=6.5$, $\alpha=0.01$). 229
- Fig. 8.11** The variation of AEP above the water table for various m subjected to different Q and corresponding to (a) $n=2.5$, $\alpha=0.01$; (b) $n=6.5$, $\alpha=0.01$; (c) $n=2.5$, $\alpha=0.005$. 232

Fig. 8.12	The variation of σ^s induced PEP component above the W.T.(z) for various m subjected to passive condition and corresponding to (a-f) $Q=0$, (g-i) $Q=-0.8$, (j-o) $Q=0.8$; (a-c, j-l) $n= 2.5$, (d-f, g-i, m-o) $n= 4$; and (a, d, g, j, m) $\alpha=0.1$, (b, e, h, k, n) $\alpha=0.01$, (c, f, i, l, o) $\alpha=0.001$.	233
Fig. 8.13	The variation of K_{ou} , K_{au} and K_{pu} above the W.T.(z) for rest- (a, d), active- (b, e) and passive – (c, f) condition respectively with a-c $\alpha = 0.01$ and d-f $\alpha = 0.005$ subjected to OPM and TPM.	237
Fig. 8.14	Schematic representation of an inclined retaining wall supporting unsaturated sloped backfills subjected to seismic forces.	239
Fig. 8.15	The impact of backfill slope (i) on the (a) critical failure angle (ζ_{cr}) and (b) area of failure wedge (A_f).	244
Fig. 8.16	The three-dimensional $K_{aue}-k_h-i$ surfaces corresponding to three different flow ratios and two values of k_v : (a) $k_v =0$, and (b) $k_v = k_h$.	246
Fig. 8.17	The variation of K_{aue} with ϕ' corresponding to various flow ratios, namely, (a, b) $Q=0$ (c, d) $Q=-0.628$, and (e, f) $Q=0.23$ and subjected to different k_v : (a,c,e) $k_v =0$, and (b,d,f) $k_v =k_h$.	247
Fig. 8.18	The variation of K_{aue} with β corresponding to various flow ratios, namely, (a, b) $Q=0$ (c, d) $Q=-0.628$, and (e, f) $Q=0.23$ and subjected to different k_v : (a,c,e) $k_v =0$, and (b,d,f) $k_v =k_h$.	249
Fig. 8.19	The variation of K_{aue} with α^{-1} corresponding to various flow ratios, namely, (a, b) $Q=0$ (c, d) $Q=-0.628$, and (e, f) $Q=0.23$ and subjected to different k_v : (a,c,e) $k_v =0$, and (b,d,f) $k_v =k_h$.	250
Fig. 8.20	The variation of K_{aue} with n considering various seismic loadings and corresponding to various flow ratios, namely, (a) $Q=0.23$, (b) $Q=0$, and (c) $Q=-0.628$.	251
Fig. 8.21	The variation of K_{aue} with h_w corresponding to various flow ratios, namely, (a, b) $Q=0$ (c, d) $Q=-0.628$, and (e, f) $Q=0.23$ and subjected to different k_v : (a,c,e) $k_v =0$, and (b,d,f) $k_v =k_h$.	253
Fig. 8.22	The variation of K_{aue} with δ considering various seismic loadings and corresponding to various flow ratios, namely, (a) $Q=0$, (b) $Q=-0.628$, and (c) $Q=0.23$.	254
Fig. 8.23	The spread of planar failure surfaces considering various seismic loadings and corresponding to (a-c) vertical wall supporting horizontal backfills and (d-f) inclined wall holding the slopy backfill.	256
Fig. 8.24	The comparison between the present solutions with the solutions reported by Rajesh and Ganesh (2022).	257
Fig. 9.1	Schematic diagram of the problem statement with the involved assumptions.	263

Fig. 9.2	Numerical scheme and the variation of matric suction with respect to time and space.	265
Fig. 9.3	Crack depth determination by plotting the variation of tensile and compressive components of total active earth pressure above the water table.	269
Fig. 9.4	The size of the Mohr circles and the Mohr failure envelopes at two different duration and two different seismic levels ($k_h=0$, $k_v=0$ and $k_h=0.2$, $k_v=0.2$) corresponding to (a-c) active and (d-f) passive state and different combinations of Q and z : (a,d) $Q=1$, $z=2$; (b,e) $Q=1$, $z=4$; and (c,f) $Q=0.2$, $z=4$.	271
Fig. 9.5	The variation of κ with respect to η for various ϕ' subjected to $Q=1$, $\alpha=0.7\text{m}^{-1}$, $z=2\text{m}$.	272
Fig. 9.6	The SWCC and the HCF profiles for the chosen hypothetical soils.	273
Fig. 9.7	The temporal variations of normalized (a, c, e) matric suction (ψ_{norm}) and (b, d, f) suction stress (σ_{norm}^s) above the water table for (a-b) clays, (c-d) silts, and (e-f) sands.	275
Fig. 9.8	Corresponding to two different spatial points and two flow ratios, the temporal variation of (a,c) σ_{norm}^s and (b,d) ψ_{norm} profiles for (a-b) silts, and (c-d) sands.	277
Fig. 9.9	Comparative study of σ_{norm}^s and ψ_{norm} profiles between the analytical solution of Shahrokhbadi et al. (2019) and numerical methods of the present study for (a, b) clay, (c, d) silt, and (e, f) sand.	278
Fig. 9.10	Comparative study of normalized active and passive earth pressure between the analytical solution of Shahrokhbadi et al. (2019) and numerical methods of the present study for (a, b) clay, (c, d) silt, and (e, f) sand.	279
Fig. 9.11	The spatial variation of normalized (a-d) AEP and (e-h) PEP profiles corresponding to (a-b, e-f) $Q=0.2$ and (c-d, g-h) $Q=1.0$ with (a,c,e,g) $k_h=0.1$, and (b,d,f,h) $k_h=0.3$.	283
Fig. 9.12	The spatial variation of normalized (a-b) AEP and (c-d) PEP profiles subjected to $Q=1$, $k_h=0.2$, and k_v equal to (a-b) $0.5 k_h$ and (b) k_h .	284
Fig. 9.13	The variation of TCD with respect to α corresponding to two different times ($t=30$ and 90 days) and subjected to various η with (a) $Q=1.0$, (b) $Q=0.2$.	285

LIST OF NOTATIONS

a_h	= Horizontal seismic acceleration
a_v	= Vertical seismic acceleration
B_i	= Integration constants
c	= Cohesive strength of homogeneous soil slope.
c_u	= Undrained cohesive strength
c_{i0}	= Undrained cohesive strength at interface
c_1	= Cohesive strength of top layer soil
c_2	= Cohesive strength of bottom layer soil
c_{eq}	= Equivalent cohesive strength of rock mass
c_r	= Reduced cohesive strength
D_f	= Disturbance factor of rock mass
D_i	= Integration constants
F_v	= Vertical seismic force
F_h	= Horizontal seismic force
F_s	= Critical factor of safety
F_{min}	= Minimum value of factor of safety
F_{max}	= Maximum value of factor of safety
f_i	= Slope surface
GSI	= Geological Strength Index
H, h	= height of slope
h_m	= Suction head
h_w	= Depth of ground water table
k_s	= Saturated hydraulic conductivity
k_r	= Relative hydraulic conductivity
k_v	= Vertical seismic acceleration coefficient
k_h	= Horizontal seismic acceleration coefficient

K_a	= Coefficient of active earth pressure for the saturated soil
K_p	= Coefficient of passive earth pressure for the saturated soil
K_{ae}	= Coefficient of seismic active earth pressure
K_{pe}	= Coefficient of seismic passive earth pressure
K_{ou}	= Coefficient of earth pressure at rest condition in the vadose zone
K_{au}	= Coefficient of active earth pressure in the vadose zone
K_{pu}	= Coefficient of passive earth pressure in the vadose zone
K_{aue}	= Seismic active earth pressure coefficient for unsaturated soil
K_{pue}	= Seismic passive earth pressure coefficient for unsaturated soil
m	= Cohesion gradient (Chapter 3)/Asymmetry parameter of vG-SWCC model (Chapter 6)
m_i	= Non-dimensional material strength parameters of intact rock mass
m_b	= The reduced value of the dimensionless material constant m_i of broken rock mass
n	= Total number of slices (Chapter 3)/Pore size distribution (Chapter 6)
N	= Stability number
N_i	= Normal force of i^{th} slice
p_{active}	= Active earth pressure
$p_{passive}$	= Passive earth pressure
p_s	= Surcharge load
Q	= Flow Ratio
q	= Surface flux
s	= Degree of fracturing of the rock mass
S_i	= Shear stress of i^{th} slice
S_e	= Effective degree of saturation
S_r	= Residual degree of saturation
t	= Time
t_{opt}	= Optimum thickness of top layer

u_a	= Pore air pressure
u_w	= Pore water pressure
W	= Self-weight of the failure soil wedge (Section 8.3.2)
W_i	= Weight of the i^{th} slice
x_0 and x_n	= Abscissas of two endpoints where the slip surface intersect with the slope surface
y_i	= Slip surface
α	= vG and Gd-SWCC model parameter
β	= Slope angle
γ	= Unit weight
γ_b	= Bulk unit weight of the soil
σ_1	= Major principal stresses
σ_3	= Minor principal stresses
σ_{ci}	= Uniaxial compressive strength of intact rock
σ'_{3max}	= Upper limit of the confining stress upto which the EMC* criterion is matched with the GHB** criterion
σ_{ni}	= Normal stress of i^{th} slice
σ_n	= Normal stress
σ^s	= Suction stress
σ^s_{norm}	= Normalized suction stress
σ^s_{avg}	= Average Suction stress
η	= Seismic intensity
η_c	= Critical seismicity
τ	= Shear strength
τ_f	= Shear stress
θ	= Volumetric water content
θ_r	= Residual volumetric water content

θ_s	= Saturation volumetric water content
θ_i	= Inclination angle of the i^{th} slice
Θ_n	= Normalized volumetric water content
ϕ	= Friction angle
ϕ_u	= Undrained friction angle
ϕ'	= Effective frictional angle
ϕ_1	= Friction angle of top layer
ϕ_2	= Friction angle of bottom layer
ϕ_{eq}	= Equivalent friction angle of rock mass
ϕ_r	= Reduced friction angle
ϕ	= Internal friction angle of homogeneous soil slope
ψ	= Matric suction
ψ_{norm}	= Normalized matric suction

*EMC= Equivalent Mohr-Coulomb Criterion,

**GHB= Generalized Hoek-Brown Criterion

LIST OF TABLES

Table No.	Title	Page No.
Table 3.1	The integral expressions of F for the corresponding cases	38
Table 3.2	The expression of the slope surfaces in the divided regions	38
Table 3.3	The expression of P_i and R_i for four cases	39
Table 3.4	The expression of A_i for four cases.	41
Table 3.5	The formulation of integration constants for four cases.	44
Table 3.6	The expression of N for four cases.	45
Table 3.7	Critical factor of safety for different slopes corresponding to different seismic coefficients	49
Table 3.8	F_s for different slopes corresponding to different seismic coefficients	52
Table 3.9	The proposed stability chart corresponding to $\phi=35^\circ$	60
Table 3.10	The proposed stability chart corresponding to $\phi=40^\circ$	61
Table 3.11	The proposed stability chart corresponding to $\phi=45^\circ$	62
Table 3.12	The Percentage improvement of F_s during the increment of ϕ from 35° to 40°	64
Table 3.13	The Percentage improvement of F_s during the increment of ϕ from 35° to 45°	65
Table 3.14	A comparison of F_s values obtained by Newmark (1965) and Choudhury et al. (2007) with the present solutions considering $k_v=0$	69
Table 3.15	A comparison of F_s values obtained from the present study with the solution of Koppula (1984) and Li et al. (2018) considering $k_h=k_v=0$ for $\beta = 45^\circ$	69
Table 3.16	A comparison of F_s values obtained from the present study with the solution of Li et al. (2018) considering $k_v=0$	70
Table 3.17	The comparison of stability number values obtained by Kumar and Samui (2006) with the present solutions considering $k_v=0$ and $c_1/c_2=1$	71
Table 3.18	A comparison of F_s values obtained from the present study with the solution of Hunter and Schuster (1968), Griffiths and Yu (2015) and Hossley and Leshchinsky (2019) considering $k_h=k_v=0$	73

Table 4.1	The values of F_s for $h= 20\text{m}$ and corresponding to different β , σ_{ci} , GSI , m_i and k_h .	90
Table 4.2	The values of F_s for $h= 100\text{m}$ and corresponding to different β , σ_{ci} , GSI , m_i and k_h .	91
Table 4.3	The values of GSI_{sp} for different β , h and σ_{ci}	95
Table 4.4	The percentage increase in F_s of the rock slope on account of the increase in σ_{ci}	97
Table 4.5	The percentage decrease in F_s of the rock slope on account of the increase in k_h	99
Table 4.6	A comparison of F_s from the present analysis with the (i) limit equilibrium solutions of Carranza-Torres (2004), and Shen et al. (2013) and (ii) limit analysis solutions of Li et al. (2011) with $k_h=0$	103
Table 4.7	A comparison of F_s from the present analysis with the (i) limit analysis solutions of Li et al. (2008) and (ii) limit equilibrium solutions of Dong-Ping et al. (2017) with $k_h=0$	103
Table 4.8	A comparison of F_s from the present analysis with the limit equilibrium solutions of Lin et al. (2014) and Huang et al. (2015) with $k_h=0$ for different GSI and m_i	105
Table 4.9	A comparison of F_s from the present analysis with the solutions of Chen and Lin (2019) obtained by using gravity increase method for $k_h=0$	106
Table 4.10	A comparison of F_s from the present analysis with the limit equilibrium solutions of Jiang et al. (2016) for 30° slope with different k_h	107
Table 5.1	The proposed stability chart (indicating the factor of safety) corresponding to $\phi_2=20^\circ$.	116
Table 5.2	The proposed stability chart (indicating the factor of safety) corresponding to $\phi_2=25^\circ$.	117
Table 5.3	The proposed stability chart (indicating the factor of safety) corresponding to $\phi_2=30^\circ$.	118
Table 5.4	A comparison of the computed lower and upper bound values of F_s for different homogeneous slopes.	126
Table 5.5	A comparison of the computed lower and upper bound values of F_s for different layered slopes.	127

Table 5.6	A comparison of F_s obtained by Dawson et al. (1999) and Chen (1975) with the present solutions for homogeneous slopes of 10 m height.	128
Table 5.7	A comparison of stability number obtained by Kumar and Samui (2006) with the present solutions in terms of stability number considering $\beta=45^\circ$ and $c_1=c_2$.	129
Table 5.8	A comparison of F_s obtained by Chatterjee and Krishna (2018) with the present solutions considering $\beta=26.57^\circ$	129
Table 5.9	A comparison of F_s obtained by Sazzad et al. (2015) with the present solutions considering $\phi_1 = \phi_2=0^\circ$ and $\beta=45^\circ$	130
Table 5.10	A comparison of F_s obtained by the variational method with the present solutions (SRM) considering $\phi_1=18^\circ$, $\phi_2=30^\circ$, and $\beta=45^\circ$	130
Table 6.1	The permissible time increment to obtain real values of m_1 and m_2 coefficient for sand ($k_s= 5.0 \times 10^{-6}$ m/s).	147
Table 6.2	The expression of B_i 's and D_i 's by considering two and three slices in Region II.	153
Table 6.3	The expression of B_i 's and D_i 's by considering four and five slices in Region II.	154
Table 6.4	The expression of B_i 's and D_i 's by dividing Region II and Region III both with two and three number of slices.	155
Table 6.5	The generalized expression of B_i 's and D_i 's for any arbitrary slicing of Regions II and III.	156
Table 6.6	A comparison of the present computed stability number (N) with the solutions presented by Vahedifard et al. (2016) and Sun et al. (2019)	173
Table 6.7	A comparison of the present solutions with the results reported by Gu et al. (2020) corresponding to different slope angle (β) and subjected to various steady-flow conditions.	174
Table 9.1	The chosen hydro-mechanical properties from previous studies (Lu and Godt 2013; Shahrokhbabadi et al. 2019).	274
Table 9.2	The computed values of TCD and $AEP_{n,gs}$ corresponding to various Q , t , and k_h .	281